LETTER

doi:10.1038/nature12041

Distinct extended amygdala circuits for divergent motivational states

Joshua H. Jennings[1,2]*, Dennis R. Sparta[1,3]*, Alice M. Stamatakis[1,2], Randall L. Ung[1], Kristen E. Pleil[3,4], Thomas L. Kash[2,3,4,5] & Garret D. Stuber[1,2,3,5,6]

The co-morbidity of anxiety and dysfunctional reward processing in illnesses such as addiction[1] and depression[2] suggests that common neural circuitry contributes to these disparate neuropsychiatric symptoms. The extended amygdala, including the bed nucleus of the stria terminalis (BNST), modulates fear and anxiety[3,4], but also projects to the ventral tegmental area (VTA)[5,6], a region implicated in reward and aversion[7–13], thus providing a candidate neural substrate for integrating diverse emotional states. However, the precise functional connectivity between distinct BNST projection neurons and their postsynaptic targets in the VTA, as well as the role of this circuit in controlling motivational states, have not been described. Here we record and manipulate the activity of genetically and neurochemically identified VTA-projecting BNST neurons in freely behaving mice. Collectively, aversive stimuli exposure produced heterogeneous firing patterns in VTA-projecting BNST neurons. By contrast, *in vivo* optically identified glutamatergic projection neurons displayed a net enhancement of activity to aversive stimuli, whereas the firing rate of identified GABAergic (γ-aminobutyric acid-containing) projection neurons was suppressed. Channelrhodopsin-2-assisted circuit mapping revealed that both BNST glutamatergic and GABAergic projections preferentially innervate postsynaptic non-dopaminergic VTA neurons, thus providing a mechanistic framework for *in vivo* circuit perturbations. *In vivo* photostimulation of BNST glutamatergic projections resulted in aversive and anxiogenic behavioural phenotypes. Conversely, activation of BNST GABAergic projections produced rewarding and anxiolytic phenotypes, which were also recapitulated by direct inhibition of VTA GABAergic neurons. These data demonstrate that functionally opposing BNST to VTA circuits regulate rewarding and aversive motivational states, and may serve as a crucial circuit node for bidirectionally normalizing maladaptive behaviours.

The ventral BNST (vBNST) is a heterogeneous structure[14] that innervates the VTA[5,15–18], and aversive and rewarding stimuli activate a subset of these vBNST projection neurons[19–21]. To identify and record the activity of vBNST–VTA neurons using antidromic photostimulation *in vivo*, we targeted channelrhodopsin-2 fused to enhanced yellow fluorescent protein (ChR2–eYFP)[22] under the control of a CaMKIIα promoter to the vBNST of adult mice. After 4–6 weeks, ChR2–eYFP was observed in vBNST cell bodies and projection fibres that innervate the VTA (Fig. 1a). Under anaesthesia, optical fibres for antidromic photostimulation were positioned above the VTA, whereas recording electrodes and optical fibres for orthodromic photostimulation were positioned in the vBNST (Fig. 1b). We recorded from vBNST units that showed reliable spiking to both orthodromic and antidromic photostimulation. By systematically decreasing the interval between orthodromic and antidromic photostimulation, the fidelity of antidromic spikes was significantly attenuated (Fig. 1c, d), demonstrating spike collision[23]. In addition, antidromic spike latencies were significantly greater and showed less variability than orthodromic spikes (Fig. 1e, f), and antidromic spike fidelity was significantly greater than orthodromic spike fidelity to 40-Hz photostimulation (Fig. 1g). Thus, photostimulation of vBNST–VTA projections results in antidromic spiking that is reliably distinguishable from putative trans-synaptic circuit activation.

To examine the neurophysiological dynamics of identified vBNST–VTA neurons in behaving mice, we implanted 16-channel multielectrode arrays in the vBNST, as well as optical fibres above the VTA for antidromic identification of neurons[24] (Fig. 1h and Supplementary Fig. 1). Delivery of single 5-ms, 473-nm light pulses to the VTA resulted in time-locked firing in many vBNST neurons. Photostimulation of vBNST–VTA fibres resulted in a bimodal firing pattern in vBNST neurons due to distinguishable antidromic and polysynaptic activity (Supplementary Fig. 2 and Methods). Principle component and correlation analysis comparing waveform shapes demonstrated that spontaneous waveforms were highly correlated with light-evoked waveforms[7] (average $r = 0.950 \pm 0.008$ (mean ± s.e.m.); Supplementary Fig. 2 and Supplementary Table 1). Light-evoked spike latencies showed that a subset of recorded units consistently displayed time-locked spiking on 11.21 ± 0.68 out of 20 trials (56%), with a mean latency of 7.31 ± 0.32 ms (Fig. 1i, j), comparable with our anaesthetized recording data (Fig. 1e) and a previous study using electrical antidromic stimulation of BNST projections in rodents[25]. Accordingly, neurons that were identified as antidromic-responsive displayed a spike fidelity of $81 \pm 15\%$ in response to 20-Hz photostimulation (Supplementary Fig. 2). Using these criteria (Methods), we identified 53 out of 137 units as vBNST–VTA projection neurons.

vBNST neurons display heterogeneous responses to aversive stimuli exposure[19,20]. Thus, we classified the firing patterns of identified vBNST–VTA neurons in response to unpredictable foot shocks and associated contextual cues (Methods). Identified vBNST–VTA neurons segregated into three functionally distinct classes based on changes in their normalized firing rates throughout the foot-shock session (Supplementary Fig. 3), demonstrating that vBNST–VTA neurons differentially encode information related to aversive stimuli and their associated contextual cues.

Electrical stimulation of the BNST produces both excitatory and inhibitory responses in VTA neurons *in vivo*[6], suggesting that distinct subcircuits may exist. Mice were injected with adeno-associated viral vector (AAV5) expressing ChR2–eYFP under the control of the CaMKIIα promoter (AAV5 CaMKIIα::ChR2–eYFP) to nonspecifically target vBNST–VTA projection neurons (CaMKIIα$^{\text{vBNST–VTA}}$::ChR2). Whole-cell recordings in brain slices revealed that photostimulation of the CaMKIIα$^{\text{vBNST–VTA}}$ pathway produced both glutamatergic and GABAergic currents in VTA neurons (Supplementary Fig. 4), demonstrating that neurochemically distinct vBNST neurons project to the VTA.

[1]Department of Psychiatry, University of North Carolina at Chapel Hill, Chapel Hill, North Carolina 27599, USA. [2]Neurobiology Curriculum, University of North Carolina at Chapel Hill, Chapel Hill, North Carolina 27599, USA. [3]Bowles Center for Alcohol Studies, University of North Carolina at Chapel Hill, Chapel Hill, North Carolina 27599, USA. [4]Department of Pharmacology, University of North Carolina at Chapel Hill, Chapel Hill, North Carolina 27599, USA. [5]Neuroscience Center, University of North Carolina at Chapel Hill, Chapel Hill, North Carolina 27599, USA. [6]Department of Cell Biology and Physiology, University of North Carolina at Chapel Hill, Chapel Hill, North Carolina 27599, USA.
*These authors contributed equally to this work.

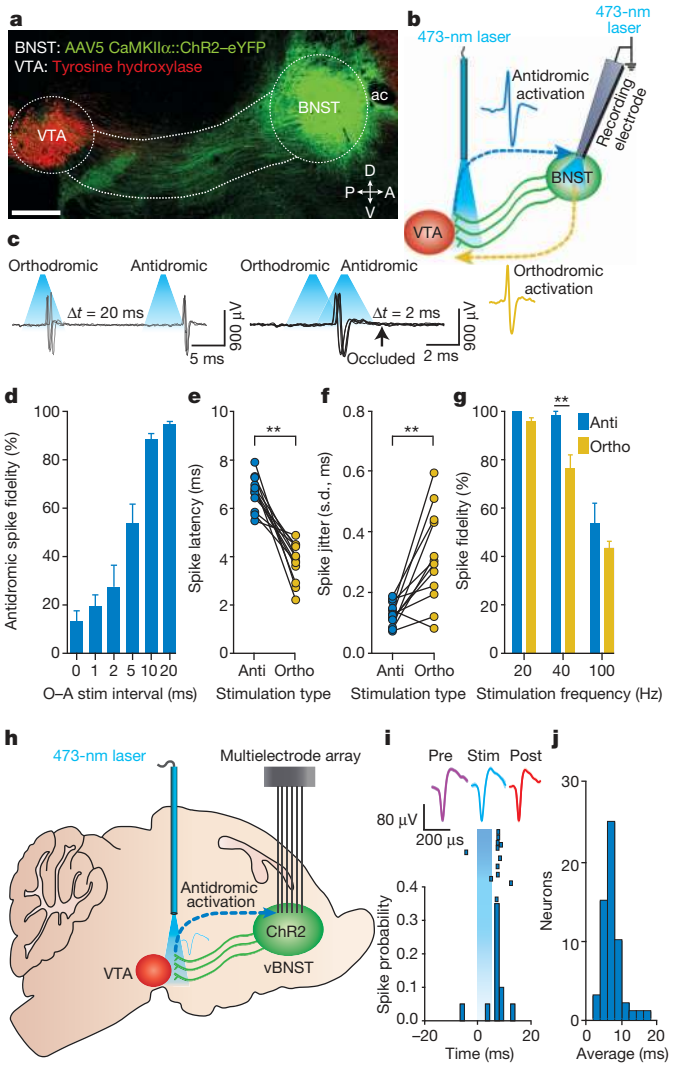

Figure 1 | Optogenetic identification of vBNST–VTA projection neurons. **a**, Sagittal image showing the vBNST–VTA projection. A, anterior; ac, anterior commissure; D, dorsal; P, posterior; V, ventral. Scale bar, 500 μm. **b**, Optogenetic collision test. **c**, Example traces from a single CaMKIIα$^{vBNST–VTA}$ unit demonstrating antidromic–orthodromic spike collision. **d**, Significant reduction in the percentage of antidromic spike fidelity at short antidromic–orthdromic (A–O) photostimulation intervals ($F_{5,65} = 48.63$, $P < 0.0001$; $n = 12$ units). **e**, Antidromic (anti) spike latencies were significantly greater than orthodromic (ortho) latencies ($P < 0.0001$; $n = 12$ units). **f**, Antidromic-initiated spikes displayed significantly greater latency stability than orthodromic-activated spikes ($P < 0.001$; $n = 12$ units). **g**, Antidromic spikes responded more reliably to 40-Hz photostimulation than orthodromic spikes ($F_{2,18} = 11.2$, $P = 0.003$, $n = 4$ units). **h**, Optogenetic identification of vBNST–VTA projection neurons in behaving mice. **i**, Representative peristimulus time histogram and raster of a single unit time-locked to 5-ms antidromic photostimulation. **j**, Mean first-spike latencies after antidromic photostimulation for all identified CaMKIIα$^{vBNST–VTA}$ projection neurons ($n = 53$ units, $n = 7$ mice). Data are mean ± s.e.m. $^{**}P < 0.01$ (Student's *t*-tests and Bonferroni post-hoc comparisons, where applicable).

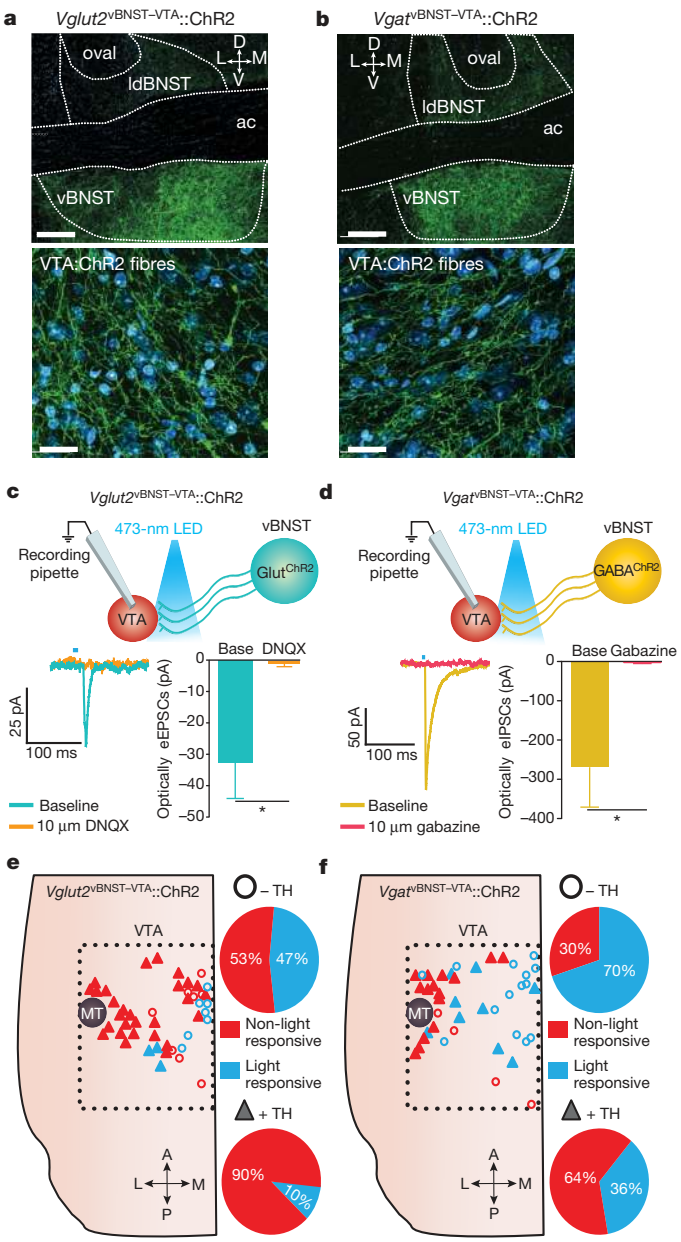

Figure 2 | Excitatory and inhibitory synapses onto non-dopaminergic VTA neurons from neurochemically distinct vBNST neurons. **a**, **b**, ChR2–eYFP (green) in the vBNST (top) and fibres in the VTA (bottom) in Vglut2-ires-cre (**a**) and Vgat-ires-cre (**b**) mice. Cyan denotes fluorescent Nissl stain. Scale bars, 200 μm (top) and 20 μm (bottom). L, lateral; ldBNST, lateral–dorsal BNST; M, medial; oval, oval nucleus BNST. **c**, Optically evoked excitatory postsynaptic currents (eEPSCs) recorded in VTA neurons after *Vglut2*$^{vBNST–VTA}$::ChR2 stimulation before and after application of the glutamate receptor antagonist 6,7-dinitroquinoxaline-2,3-dione (DNQX) (bottom) ($n = 4$ cells, $P = 0.0307$). LED, light-emitting diode. **d**, Optically evoked inhibitory postsynaptic currents (eIPSCs) recorded in VTA neurons after *Vgat*$^{vBNST–VTA}$::ChR2 stimulation before and after application of the $GABA_A$ receptor antagonist gabazine (bottom) ($n = 4$ cells, $P = 0.0378$). **e**, **f**, Location of light-responsive and non-light-responsive dopaminergic and non-dopaminergic neurons in horizontal VTA slices after photostimulation of *Vglut2*$^{vBNST–VTA}$::ChR2 (**e**) and *Vgat*$^{vBNST–VTA}$::ChR2 (**f**) projections. TH, tyrosine hydroxylase. Data are mean ± s.e.m. $^{*}P < 0.05$ (Student's *t*-test for paired samples).

We next dissected the functional connectivity between distinct glutamatergic and GABAergic vBNST–VTA neurons and their genetically defined postsynaptic targets within the VTA. Injection of a Cre-inducible viral construct coding for ChR2–eYFP into the vBNST in Vglut2-ires-cre or Vgat-ires-cre mouse lines (which express Cre recombinase from the endogenous *Vglut2* (also known as *Slc17a6*) or *Vgat* (*Slc32a1*) promoters, respectively)[26] resulted in robust expression in the vBNST as well as in fibres originating from these neurons that innervated the VTA (Fig. 2a, b). Whole-cell recordings from VTA neurons revealed that photostimulation of ChR2-containing fibres originating from vBNST neurons expressing *Vglut2* (*Vglut2*$^{vBNST–VTA}$::ChR2) or *Vgat* (*Vgat*$^{vBNST–VTA}$::ChR2) produced excitatory or inhibitory postsynaptic currents, respectively (Fig. 2c, d and Supplementary Fig. 5). *Vglut2*$^{vBNST–VTA}$ and *Vgat*$^{vBNST–VTA}$ terminals formed functional

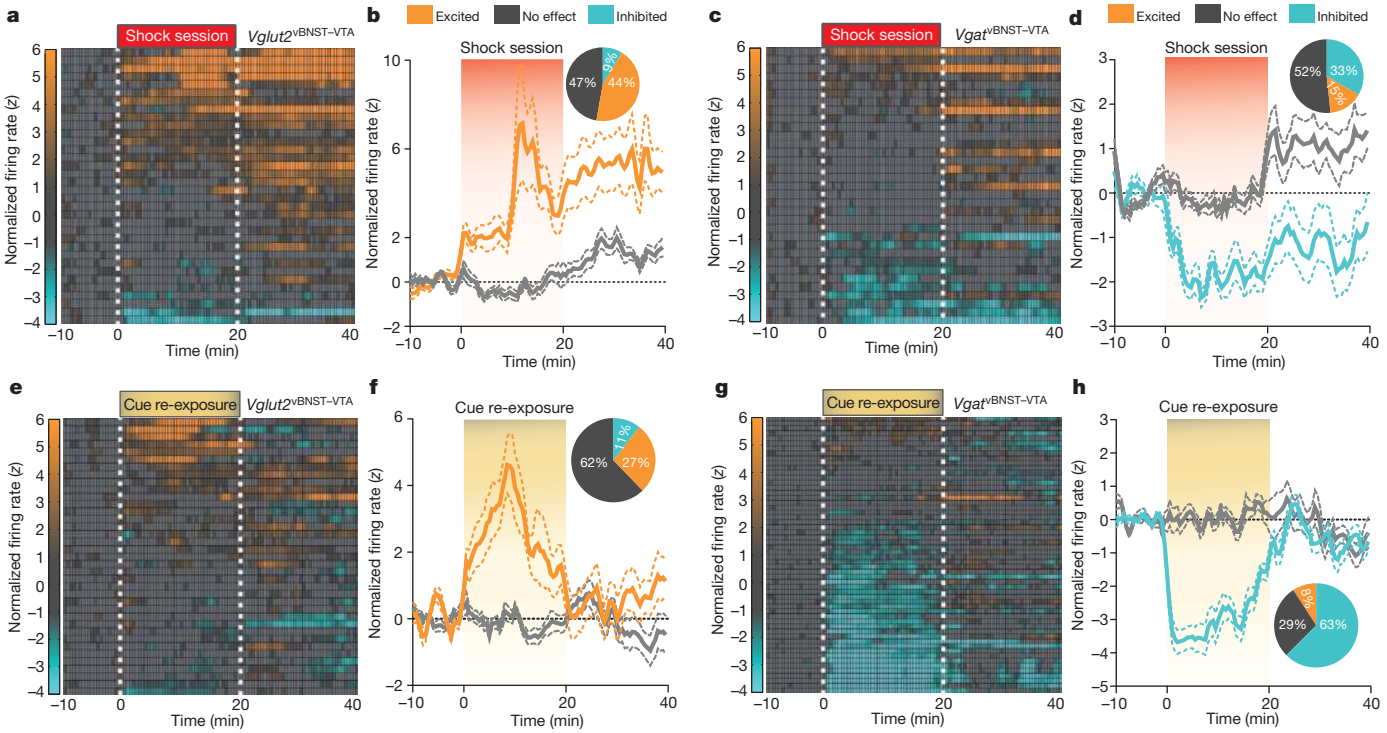

Figure 3 | *Vglut2*$^{vBNST–VTA}$ and *Vgat*$^{vBNST–VTA}$ projection neurons display distinct firing patterns in response to foot-shock and shock-associated contextual cues. **a**, Colour-coded normalized firing rates for all identified *Vglut2*$^{vBNST–VTA}$ neurons in response to the first foot-shock session. **b**, Average normalized firing rate of classified shock-excited *Vglut2*$^{vBNST–VTA}$ neurons is significantly altered compared to classified no-effect neurons during and after the foot-shock session ($F_{99,2900} = 3.13$, $P < 0.0001$, $n = 34$ units, $n = 7$ mice). Inset, percentages of classified neurons. **c**, Colour-coded normalized firing rates for all identified *Vgat*$^{vBNST–VTA}$ neurons in response to the first foot-shock session. **d**, Average normalized firing rate of classified shock-inhibited *Vgat*$^{vBNST–VTA}$ neurons is significantly altered compared to classified no-effect neurons during and after the foot-shock session ($F_{99,2600} = 2.66$, $P < 0.0001$, $n = 33$ units, $n = 5$ mice). **e**, Colour-coded normalized firing rates of identified *Vglut2*$^{vBNST–VTA}$ neurons in response to cue re-exposure. **f**, Average normalized firing rate of classified cue-excited *Vglut2*$^{vBNST–VTA}$ neurons is significantly altered compared to classified no-effect neurons during and after cue re-exposure ($F_{99,3100} = 5.135$, $P < 0.0001$, $n = 37$ units, $n = 4$ mice). **g**, Colour-coded normalized firing rates of *Vgat*$^{vBNST–VTA}$ neurons in response to cue re-exposure. **h**, Average normalized firing rate of classified cue-inhibited *Vgat*$^{vBNST–VTA}$ neurons is significantly altered compared to classified no-effect neurons during and after cue re-exposure ($F_{99,4,900} = 8.285$, $P < 0.0001$, $n = 56$ units, $n = 4$ mice).

synapses primarily onto non-dopaminergic and medially located dopaminergic neurons, which have been implicated in responding to aversive stimuli[7,9,11,13] (Fig. 2e, f and Supplementary Figs 6 and 7 and Methods). These data provide a circuit blueprint by which vBNST subcircuits interact with VTA-reward circuitry.

We next explored whether glutamatergic or GABAergic subpopulations of vBNST–VTA neurons differentially respond to foot-shock sessions and associated contextual cues. Using optical antidromic activation *in vivo*, we identified 34 *Vglut2*$^{vBNST–VTA}$::ChR2-expressing neurons out of 145 recorded neurons (Supplementary Figs 1 and 8 and Supplementary Table 1). Although all projection neurons displayed heterogeneous firing patterns (Supplementary Fig. 3), identified *Vglut2*$^{vBNST–VTA}$ projection neurons exhibited a net enhancement of firing during the aversive event (Fig. 3a, b). By contrast, 33 identified *Vgat*$^{vBNST–VTA}$::ChR2-expressing neurons out of 77 total neurons principally exhibited reduced firing during the aversive event (Fig. 3c, d, Supplementary Figs 1 and 8 and Supplementary Table 1). In addition, 1 week after five consecutive daily foot-shock sessions, re-exposure to shock-associated contextual cues alone resulted in a net enhancement of *Vglut2*$^{vBNST–VTA}$::ChR2 neuronal activity (Fig. 3e, f and Supplementary Fig. 9), whereas the activity of *Vgat*$^{vBNST–VTA}$::ChR2 neurons was largely suppressed (Fig. 3g, h and Supplementary Fig. 9). Collectively, exposure to the aversive event or associated cues alone enhanced the firing of *Vglut2*$^{vBNST–VTA}$ neurons, while simultaneously suppressing the activity of *Vgat*$^{vBNST–VTA}$ neurons.

Because aversive stimuli enhanced the activity of *Vglut2*$^{vBNST–VTA}$ neurons (Fig. 3a, b, e, f), which can excite non-dopaminergic VTA neurons (Fig. 2e), we next explored the behavioural consequences of selectively activating this projection in behaving mice. We tested mice in a real-time place preference (RTPP) model to assay the effects of photostimulation of the *Vglut2*$^{vBNST–VTA}$ pathway on motivational valence. Photostimulation of *Vglut2*$^{vBNST–VTA}$::ChR2 mice resulted in a significant avoidance of a stimulation-paired chamber (Fig. 4a, b and Supplementary Figs 10 and 11). Activation of this pathway also reduced active reward seeking (Supplementary Fig. 11). The aversive effects of this stimulation was dependent on local VTA glutamatergic signalling as infusions of an ionotropic glutamate receptor antagonist cocktail abolished the aversive phenotype induced by *Vglut2*$^{vBNST–VTA}$ activation (Fig. 4b and Supplementary Figs 12 and 13). In addition, inescapable activation of this pathway for 20 min in an open field resulted in significantly less centre and more corner time in *Vglut2*$^{vBNST–VTA}$::ChR2 mice in the 10 min after stimulation offset compared to controls, suggesting that enhanced activity in the *Vglut2*$^{vBNST–VTA}$ pathway contributes to anxiety-like behaviour (Fig. 4c and Supplementary Fig. 11).

In contrast to the aversive consequences of stimulating the *Vglut2*$^{vBNST–VTA}$ pathway, 20-Hz photostimulation in *Vgat*$^{vBNST–VTA}$::ChR2 mice resulted in a significant place preference (Fig. 5a, b and Supplementary Figs 10 and 14). VTA infusions of a $GABA_A$ receptor antagonist prevented the *Vgat*$^{vBNST–VTA}$-mediated place preference compared to saline injections (Fig. 5b and Supplementary Figs 12 and 13). To determine whether *in vivo* optogenetic activation of the *Vgat*$^{vBNST–VTA}$ pathway produces active reward seeking, we tested whether these mice would nose poke to receive photostimulation[27]. *Vgat*$^{vBNST–VTA}$::ChR2 mice readily nose poked to receive photostimulation (Fig. 5c and Supplementary Fig. 14). Together, these data suggest

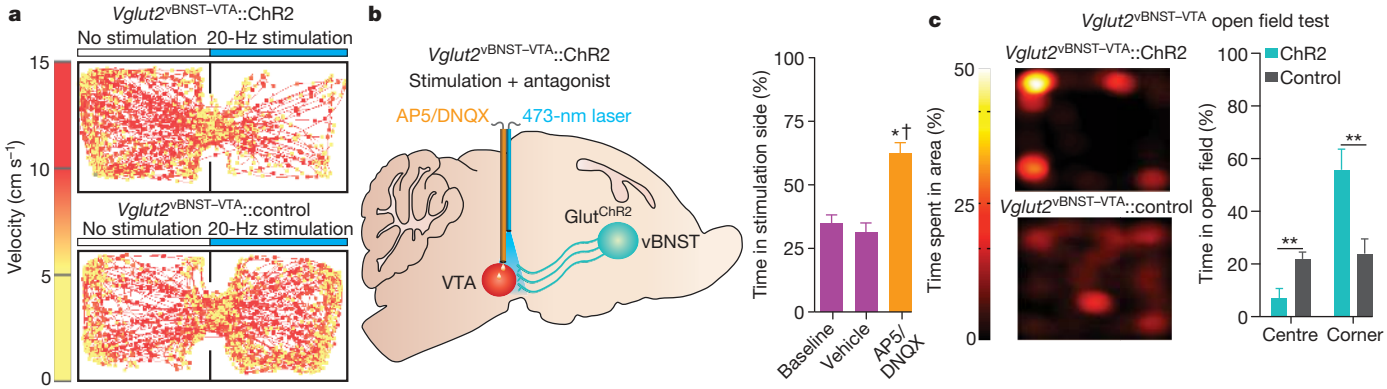

Figure 4 | Photostimulation of the *Vglut2*$^{vBNST–VTA}$ pathway promotes aversion and anxiety. **a**, Representative RTPP tracks from *Vglut2*$^{vBNST–VTA}$::ChR2 (top) and control (bottom) mice. **b**, Intra-VTA infusions of a glutamate antagonist cocktail (D(−)-2-amino-5-phosphonovaleric acid (AP5) plus DNQX), followed by *Vglut2*$^{vBNST–VTA}$::ChR2 stimulation during blocked aversion in the RTPP test ($F_{3,15} = 12.811$, $P < 0.001$, $n = 6$ mice). **c**, Representative heat maps displaying average time spent in an open field for 10 min after stimulation from *Vglut2*$^{vBNST–VTA}$::ChR2 (top) and *Vglut2*$^{vBNST–VTA}$::control (bottom) mice. *Vglut2*$^{vBNST–VTA}$::ChR2 mice spent significantly more time in the corners ($P = 0.008$) and less time in the centre ($P = 0.007$) of an open field immediately after constant 20-Hz stimulation than *Vglut2*$^{vBNST–VTA}$::control mice ($n = 6$ mice per group). Data are mean ± s.e.m. $*P < 0.05$; $**P < 0.01$. Dagger symbol denotes significance compared to all manipulations.

that photostimulation of the *Vgat*$^{vBNST–VTA}$ pathway promotes reward-related behaviours.

Because the *Vgat*$^{vBNST–VTA}$ projection preferentially innervates non-dopaminergic VTA neurons (Fig. 2f), we considered VTA GABAergic neurons as the likely postsynaptic target. VTA GABAergic neuronal inhibition via halorhodopsin activation with enhanced *Natronomonas pharaonis* halorhodopsin (eNpHR3.0) (Supplementary Figs 15 and 16) also produced reward-related phenotypes (*Vgat*^{VTA}::eNpHR3.0;

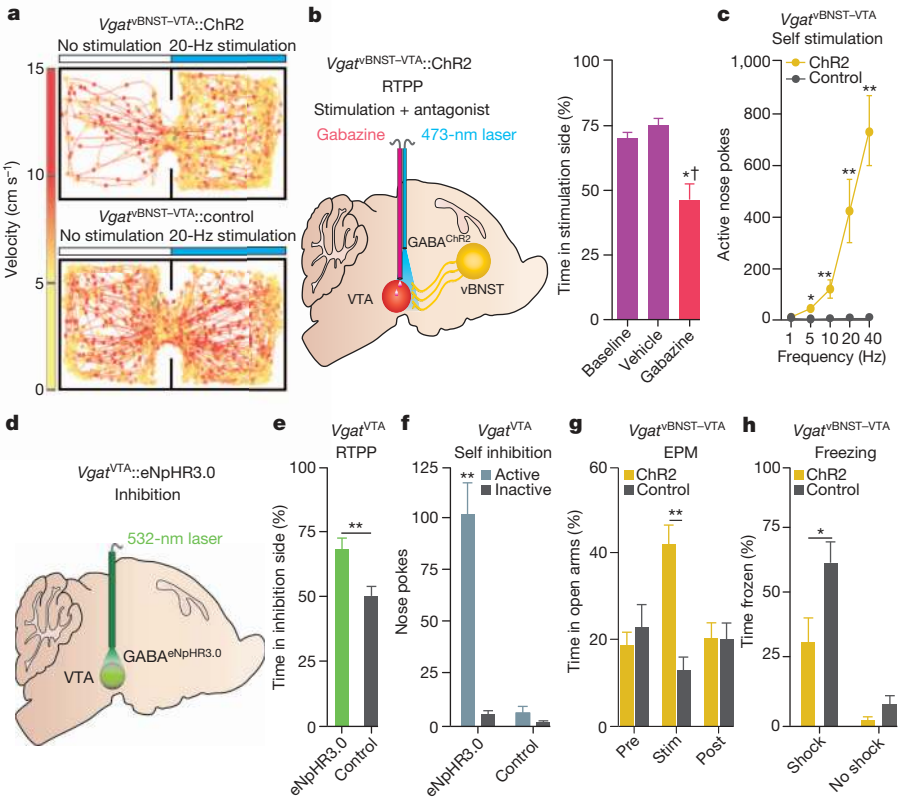

Figure 5 | Photostimulation of the *Vgat*$^{vBNST–VTA}$ pathway and inhibition of *Vgat*^{VTA} neurons produces reward-related behaviours and attenuates anxiety. **a**, Representative RTPP tracks from *Vgat*$^{vBNST–VTA}$::ChR2 (top) and control (bottom) mice. **b**, Intra-VTA infusions of the $GABA_A$ antagonist gabazine followed by *Vgat*$^{vBNST–VTA}$::ChR2 stimulation abolished place preference ($F_{3,15} = 13.718$, $P < 0.001$, $n = 6$ mice). **c**, *Vgat*$^{vBNST–VTA}$::ChR2 mice made significantly more nose pokes to obtain photostimulation than controls ($F_{4,36} = 12.42$, $P < 0.001$, $n = 5–7$ mice per group). **d**, Schematic detailing *Vgat*^{VTA}::eNpHR3.0 inhibition during behavioural experiments. **e**, *Vgat*^{VTA}::eNpHR3.0 mice spent significantly more time in the inhibition-paired side than controls ($P = 0.01$, $n = 6$ mice per group). **f**, *Vgat*^{VTA}::eNpHR3.0 mice made significantly more nose pokes to obtain photoinhibition than controls ($P < 0.001$, $n = 5$ mice per group). **g**, *Vgat*$^{vBNST–VTA}$::ChR2 mice spent significantly more time in the EPM open arms than controls during the 5-min photostimulation epoch ($F_{2,24} = 14.648$, $P < 0.001$, $n = 7$ mice per group). **h**, After concurrent photostimulation during the foot-shock session, *Vgat*$^{vBNST–VTA}$::ChR2 mice ($n = 6–7$) spent significantly less time frozen than controls ($F_{1,22} = 37.992$, $P < 0.001$). Data are mean ± s.e.m. $*P < 0.05$; $**P < 0.01$. Dagger symbol denotes significance compared to all manipulations.

Fig. 5d–f). Together, these results show that reward-related responses to $Vgat^{vBNST–VTA}$ activation are recapitulated by directly inhibiting $Vgat^{VTA}$ neurons, thus providing a circuit mechanism for the $Vgat^{vBNST–VTA}$ pathway to regulate motivated behaviour.

As the BNST regulates the expression of fear and anxiety-related behavioural phenotypes[3,28,29], we also sought to establish a role for the $Vgat^{vBNST–VTA}$ pathway in these negative motivational states. Photostimulation of the $Vgat^{vBNST–VTA}$ pathway and direct inhibition of $Vgat^{VTA}$ neurons significantly increased the time spent in the open arms of an elevated-plus maze (EPM) test, indicative of anxiolysis (Fig. 5g and Supplementary Fig. 17). These coinciding observations suggest that $Vgat^{vBNST–VTA}$ and $Vgat^{VTA}$ neurons act as crucial circuit nodes for moderating the expression of anxiety.

Given that $Vgat^{vBNST–VTA}$ neurons are largely inhibited by aversive stimuli (Fig. 3c, d, g, h), we examined whether concurrent activation of the $Vgat^{vBNST–VTA}$ projection during an unpredictable foot-shock session could alleviate the subsequent development of anxiety-like behaviour. Immediately after termination of the foot-shock session and cessation of $Vgat^{vBNST–VTA}$::ChR2 stimulation, we measured the acute freezing response while mice were still in the shock-associated context, as well as their behaviour in the EPM test 3 h later (Supplementary Fig. 18 and Methods). $Vgat^{vBNST–VTA}$::ChR2 mice spent significantly less time frozen (Fig. 5h), as well as significantly more open-arm time and entries in the EPM test relative to controls (Supplementary Fig. 18). Taken together, these data suggest that enhancing activity of the $Vgat^{vBNST–VTA}$ pathway during aversive stimuli exposure has anxiety-buffering properties. Although the canonical view of BNST function proposes a dominant role of this structure in promoting anxiety states[3,4,30], the cellular and functional complexity described here (Supplementary Fig. 19) illustrates that particular BNST circuit elements orchestrate divergent aspects of emotional and motivational processing.

METHODS SUMMARY

All procedures were conducted in accordance with the Guide for the Care and Use of Laboratory Animals, as adopted by the National Institutes of Health, and with approval of the Institutional Animal Care and Use Committee at the University of North Carolina and described in detail in the Methods.

Full Methods and any associated references are available in the online version of the paper.

Received 7 September 2012; accepted 25 February 2013.
Published online 20 March 2013.

1. Koob, G. F. & Le Moal, M. Drug addiction, dysregulation of reward, and allostasis. *Neuropsychopharmacology* **24,** 97–129 (2001).
2. Nestler, E. J. & Carlezon, W. A. Jr. The mesolimbic dopamine reward circuit in depression. *Biol. Psychiatry* **59,** 1151–1159 (2006).
3. Davis, M., Walker, D. L., Miles, L. & Grillon, C. Phasic vs sustained fear in rats and humans: role of the extended amygdala in fear vs anxiety. *Neuropsychopharmacology* **35,** 105–135 (2010).
4. Walker, D. L. & Davis, M. Role of the extended amygdala in short-duration versus sustained fear: a tribute to Dr. Lennart Heimer. *Brain Struct. Funct.* **213,** 29–42 (2008).
5. Geisler, S. & Zahm, D. S. Afferents of the ventral tegmental area in the rat-anatomical substratum for integrative functions. *J. Comp. Neurol.* **490,** 270–294 (2005).
6. Georges, F. & Aston-Jones, G. Potent regulation of midbrain dopamine neurons by the bed nucleus of the stria terminalis. *J. Neurosci.* **21,** RC160 (2001).
7. Cohen, J. Y., Haesler, S., Vong, L., Lowell, B. B. & Uchida, N. Neuron-type-specific signals for reward and punishment in the ventral tegmental area. *Nature* **482,** 85–88 (2012).
8. Fields, H. L., Hjelmstad, G. O., Margolis, E. B. & Nicola, S. M. Ventral tegmental area neurons in learned appetitive behavior and positive reinforcement. *Annu. Rev. Neurosci.* **30,** 289–316 (2007).
9. Lammel, S. *et al.* Input-specific control of reward and aversion in the ventral tegmental area. *Nature* **491,** 212–217 (2012).
10. Stamatakis, A. M. & Stuber, G. D. Activation of lateral habenula inputs to the ventral midbrain promotes behavioral avoidance. *Nature Neurosci.* **15,** 1105–1107 (2012).
11. Tan, K. R. *et al.* GABA neurons of the VTA drive conditioned place aversion. *Neuron* **73,** 1173–1183 (2012).
12. Tye, K. M. *et al.* Dopamine neurons modulate neural encoding and expression of depression-related behaviour. *Nature* **493,** 537–541 (2012).
13. van Zessen, R., Phillips, J. L., Budygin, E. A. & Stuber, G. D. Activation of VTA GABA neurons disrupts reward consumption. *Neuron* **73,** 1184–1194 (2012).
14. Hammack, S. E., Mania, I. & Rainnie, D. G. Differential expression of intrinsic membrane currents in defined cell types of the anterolateral bed nucleus of the stria terminalis. *J. Neurophysiol.* **98,** 638–656 (2007).
15. Dong, H. W. & Swanson, L. W. Organization of axonal projections from the anterolateral area of the bed nuclei of the stria terminalis. *J. Comp. Neurol.* **468,** 277–298 (2004).
16. Dumont, E. C. & Williams, J. T. Noradrenaline triggers GABAA inhibition of bed nucleus of the stria terminalis neurons projecting to the ventral tegmental area. *J. Neurosci.* **24,** 8198–8204 (2004).
17. Jalabert, M., Aston-Jones, G., Herzog, E., Manzoni, O. & Georges, F. Role of the bed nucleus of the stria terminalis in the control of ventral tegmental area dopamine neurons. *Prog. Neuropsychopharmacol. Biol. Psychiatry* **33,** 1336–1346 (2009).
18. Kudo, T. *et al.* Three types of neurochemical projection from the bed nucleus of the stria terminalis to the ventral tegmental area in adult mice. *J. Neurosci.* **32,** 18035–18046 (2012).
19. Briand, L. A., Vassoler, F. M., Pierce, R. C., Valentino, R. J. & Blendy, J. A. Ventral tegmental afferents in stress-induced reinstatement: the role of cAMP response element-binding protein. *J. Neurosci.* **30,** 16149–16159 (2010).
20. Christianson, J. P. *et al.* Safety signals mitigate the consequences of uncontrollable stress via a circuit involving the sensory insular cortex and bed nucleus of the stria terminalis. *Biol. Psychiatry* **70,** 458–464 (2011).
21. Mahler, S. V. & Aston-Jones, G. S. Fos activation of selective afferents to ventral tegmental area during cue-induced reinstatement of cocaine seeking in rats. *J. Neurosci.* **32,** 13309–13325 (2012).
22. Boyden, E. S., Zhang, F., Bamberg, E., Nagel, G. & Deisseroth, K. Millisecond-timescale, genetically targeted optical control of neural activity. *Nature Neurosci.* **8,** 1263–1268 (2005).
23. Fuller, J. H. & Schlag, J. D. Determination of antidromic excitation by the collision test: problems of interpretation. *Brain Res.* **112,** 283–298 (1976).
24. Sparta, D. R. *et al.* Construction of implantable optical fibers for long-term optogenetic manipulation of neural circuits. *Nature Protocols* **7,** 12–23 (2012).
25. Nagy, F. Z. & Pare, D. Timing of impulses from the central amygdala and bed nucleus of the stria terminalis to the brain stem. *J. Neurophysiol.* **100,** 3429–3436 (2008).
26. Vong, L. *et al.* Leptin action on GABAergic neurons prevents obesity and reduces inhibitory tone to POMC neurons. *Neuron* **71,** 142–154 (2011).
27. Stuber, G. D. *et al.* Excitatory transmission from the amygdala to nucleus accumbens facilitates reward seeking. *Nature* **475,** 377–380 (2011).
28. Erb, S., Shaham, Y. & Stewart, J. Stress-induced relapse to drug seeking in the rat: role of the bed nucleus of the stria terminalis and amygdala. *Stress* **4,** 289–303 (2001).
29. Poulos, A. M., Ponnusamy, R., Dong, H. W. & Fanselow, M. S. Compensation in the neural circuitry of fear conditioning awakens learning circuits in the bed nuclei of the stria terminalis. *Proc. Natl Acad. Sci. USA* **107,** 14881–14886 (2010).
30. Phelps, E. A. & LeDoux, J. E. Contributions of the amygdala to emotion processing: from animal models to human behavior. *Neuron* **48,** 175–187 (2005).

Supplementary Information is available in the online version of the paper.

Acknowledgements We thank M. Patel, J. Phillips and S. Maciver for assistance; V. Gukassyan and the UNC Neuroscience Center Microscopy Core (P30 NS045892), and members of the Stuber laboratory for discussion. We thank K. Deisseroth for viral constructs and the UNC Vector Core Facility for viral packaging. We thank B. Lowell and L. Vong for providing the Vgat-ires-cre and Vglut2-ires-cre mice. This study was supported by The Whitehall Foundation, The Foundation of Hope, National Institutes of Health grants DA029325 and DA032750 (to G.D.S.), AA018610 and AA007573 (to D.R.S.), NS007431 and DA034472 (to A.M.S.) and AA021043 (to K.P.), and the UNC NIAAA alcohol research center (AA011605).

Author Contributions D.R.S., J.H.J. and G.D.S. designed all experiments and wrote the manuscript. All authors collected, analysed and discussed the data.

Author Information Reprints and permissions information is available at www.nature.com/reprints. The authors declare no competing financial interests. Readers are welcome to comment on the online version of the paper. Correspondence and requests for materials should be addressed to G.D.S. (gstuber@med.unc.edu).

METHODS

Experimental subjects and stereotactic surgery. All procedures were conducted in accordance with the Guide for the Care and Use of Laboratory Animals, as adopted by the National Institutes of Health, and with approval of the Institutional Animal Care and Use Committee at the University of North Carolina (UNC). Adult (25–30 g) male C57BL/6J mice (Jackson Laboratory), adult male Vgat-ires-cre mice and adult male Vglut2-ires-cre mice (see ref. 26 for further details on the Vglut2-ires-cre and Vgat-ires-cre mouse lines) were group-housed before surgery. All mice were maintained on a reverse 12-h light cycle (lights off at 7:00) with *ad libitum* access to food and water, unless described otherwise. Mice were anaesthetized with a ketamine (150 mg per kg of body weight) and xylazine (50 mg per kg) solution and placed into a stereotactic frame (Kopf Instruments). For all *in vivo* electrophysiology experiments, male mice were unilaterally injected with 0.5 µl of purified and concentrated adeno-associated virus (AAV) ($\sim 10^{12}$ infections units per ml, packaged by the UNC Vector Core Facility) into the vBNST using the following stereotactic coordinates: +0.14 mm to bregma, ±0.9 mm lateral to midline, and −4.8 mm ventral to the skull surface. All viral constructs were packaged by the UNC Vector Core Facility at a final working concentration of 1×10^{12}–5×10^{12} genome copies per millilitre.

For all *in vivo* electrophysiology experiments, mice were implanted with a 16-wire (4 × 4 configuration, wire diameter ~30 µm) tungsten multielectrode array (Innovative Neurophysiology) aimed at the vBNST using the stereotactic coordinates stated above. For all *in vivo* electrophysiological and behavioural experiments, except for the VTA microinjection experiments, all mice were implanted with an optical fibre aimed at the VTA (see ref. 24 for further details), using the following stereotactic coordinates: −3.2 mm to bregma, ±0.5 mm lateral to midline, and −4.69 mm ventral to the skull surface. For the VTA microinjection experiments, a 26-gauage steel tube cannula (McMasters-Carr) that terminated 0.5 mm above the tip of the optical fibre was epoxied to an optical fibre and unilaterally aimed at the VTA using the following stereotactic coordinates: −3.2 mm to bregma, ±0.5 mm lateral to midline, and −4.69 mm ventral to skull surface. For photoinhibition of VTA-GABAergic neurons using eNpHR3.0, all mice were bilaterally implanted with an optical fibre at a 10° angle in the VTA using the following stereotactic coordinates: −3.2 mm to bregma, ±1.1 mm lateral to midline, and −4.75 mm ventral to the skull surface. The time from virus injection to the start of the experiments was 4–6 weeks for all ChR2 terminal stimulation manipulations, and 3–4 weeks for cell body manipulations.

Histology, immunohistochemistry and microscopy. Mice were anaesthetized with pentobarbital, and transcardially perfused with PBS followed by 4% (w/v) paraformaldehyde in PBS. Forty-micrometre brain sections were subjected to immunohistochemical staining for neuronal cell bodies (NeuroTrace Invitrogen; 640 nm excitation/660 nm emission or 435 nm excitation/455 nm emission and/or tyrosine hydroxylase) (Pel Freeze; made in sheep, 1:500) (see refs 10, 13 for additional information). Brain sections were mounted, coverslips added, and *z*-stack and tiled images were captured on a Zeiss LSM 710 confocal microscope using a ×20 or ×63 objective. To determine optical fibre placement, tissue was imaged at ×10 and ×20 on an upright epi-fluorescent microscope.

***In vivo* anaesthetized electrophysiology.** C57BL/6J mice were bilaterally injected with 0.3 µl of AAV5 CaMKIIα::ChR2–eYFP into the vBNST. Six weeks after virus injection, mice were anaesthetized with 0.5–1.0% isoflurane (Butler Schein) and were placed into a stereotaxic frame (Kopf Instruments). Body temperature was maintained at ~37 °C with a homeothermic heating blanket (Harvard Apparatus). Tail pinches were administered frequently to monitor responses under anaesthesia. A reference electrode was fixed inside brain tissue, approximately 2 mm from both the vBNST and VTA. Extracellular neural activity was recorded using a glass recording electrode (5–10 MΩ: and filled with 0.5 M NaCl). The recording electrode was lowered into the vBNST (+0.14 mm to bregma, ±0.9 mm lateral to midline, and −4.8 mm ventral to the skull surface) by a motorized micromanipulator (Scientifica). Recordings were amplified (Multiclamp 700B, Molecular Devices), high-pass filtered at 6 kHz and sampled at 10 kHz. Here, orthodromic photostimulation refers to action potentials initiated at the cell body, whereas antidromic photostimulation refers to backward propagating action potentials initiated at distal axonal fibres; both are independent of synaptic transmission.

For orthodromic activation, an optical fibre coupled to a solid state laser (473 nm) was fed through the side port of the electrode holder to terminate near the tip of the glass recording electrode, which allowed for delivery of ~5 mW light pulses into the vBNST. For antidromic activation, an optical fibre housed in a steel cannula and coupled to a separate solid-state laser (473 nm) was inserted into the VTA at a 16° angle (−3.2 mm to bregma, +1.4 mm lateral to midline, and −4.9 mm ventral to the skull surface), which delivered ~10 mW of light to the VTA. vBNST neurons were classified as antidromic-responsive if the following three criteria were met: (1) stable antidromic spike latency (<0.2 ms); (2) ability to respond reliably to high-frequency photostimulation; and (3) collision between orthodromic- and antidromic-evoked spikes. Each photostimulation parameter delivered a 5-ms light pulse to either vBNST cell bodies (orthodromic) or vBNST axons within the VTA (antidromic). To determine stable antidromic latencies, 5-ms light pulses were delivered to the VTA every 5 s for 20 trials. To confirm reliable antidromic spike fidelity, 20-, 40- and 100-Hz train pulses of light were delivered to the VTA every 10 s for 10 trials at each frequency. To validate spike collision, we varied the collision interval (0, 1, 2, 5, 10 and 20 ms) between orthodromic and antidromic photostimulation. Each collision interval was repeated every 5 s for a total of 10 trials. Data acquisition and analysis was performed using pCLAMP software (Molecular Devices). Placements of recording electrode tips within the vBNST and optical fibres within the VTA were verified with histological examination of brain tissue after the experiments.

Patch-clamp electrophysiology. Brain slices preparation and general methods for patch-clamp electrophysiology were conducted as previously described[10,13], with the following changes. To examine both vBNST postsynaptic glutamatergic and GABAergic currents, C57BL/6J mice were injected with AAV5 CaMKIIα::ChR2–eYFP to nonspecifically target vBNST–VTA projection neurons ($CaMKII\alpha^{vBNST-VTA}$::ChR2). For whole-cell voltage recordings (EPSCs and IPSCs) from VTA neurons, electrodes (2–4 MΩ electrode resistance) contained (in mM): 117 caesium methanesulphonate, 20 HEPES, 0.4 EGTA, 2.8 NaCl, 5 TEA, 2 Mg-ATP, 0.2 Na-GTP, pH 7.2–7.4, 275–285 mOsm. The caesium methanesulphonate internal solution also contained the selective NMDA (*N*-methyl-D-aspartate) antagonist MK-801 (1.125 mM). VTA neurons were clamped at holding potential (V_h) of −70 mV (reversal potential (E_{rev}) for $GABA_A$ receptors) and +10 mV (E_{rev} for AMPA (α-amino-3-hydroxy-5-methyl-4-isoxazole propionic acid) receptors) to examine both glutamatergic and GABAergic postsynaptic currents, respectively, within the same neuron. Photostimulation (5-ms pulses of 1–2 mW, 473-nm light delivery via LED through a ×40 microscope objective) was used at both voltages. In a subset of neurons ($n = 4$ of 11 neurons), tetrodotoxin (1 µM) and 4-aminopyridine (1 mM) were bath-applied to isolate monosynaptic currents.

To isolate vBNST glutamatergic and GABAergic postsynaptic currents, $Vglut2^{vBNST-VTA}$::ChR2 and $Vgat^{vBNST-VTA}$::ChR2 mice were used for recordings. For whole-cell voltage-clamp recordings of VTA EPSCs from $Vglut2^{vBNST-VTA}$::ChR2 mice, once stable light-evoked EPSCs were achieved, 10 µM DNQX was bath-applied. For whole-cell voltage-clamp recordings of VTA IPSCs from $Vgat^{vBNST-VTA}$::ChR2 mice, once stable light-evoked IPSCs were achieved, 10 µM gabazine was bath-applied.

***Ex vivo* validation of photoinhibition of VTA GABA neurons.** For current clamp recordings to show hyperpolarization of membrane voltage from VTA GABA neurons after eNpHR3.0 inhibition, Vgat-ires-cre mice were transduced with Cre-inducible eNpHR3.0 under the control of the EF1α promoter in the VTA. Electrodes (2–4 MΩ) contained (in mM): 130 K-gluconate, 10 KCl, 10 HEPES, 10 EGTA, 2 $MgCl_2$, 2 Mg-ATP, 0.2 Na-GTP, pH 7.2–7.4, 275–285 mOsm. VTA neurons were maintained at ~60 mV. For photoinhibition, 500-ms pulses of 5–8-mW, 532-nm light delivery via a solid-state laser coupled to an optical fibre positioned in the brain slice.

Unpredictable foot-shock model. Mice were placed in sound-attenuated mouse behavioural chambers (Med Associates), where an unpredictable foot shock was used as an aversive stimulus. A house light and white noise signalled the start of the trial and remained on throughout the entire 20-min foot-shock session (contextual cues). Each unpredictable foot shock was 0.75 mA in intensity and 500 ms in duration on a variable interval (VI60) schedule. Mice received approximately 20 unpredictable foot shocks during the entire 20-min session.

For the *in vivo* electrophysiology experiments, $Vglut2^{vBNST-VTA}$::ChR2 and $Vgat^{vBNST-VTA}$::ChR2 mice implanted with a multielectrode array in the vBNST and an optical fibre in the VTA were placed in the unpredictable foot-shock context in which they received the visual and auditory contextual cues in the absence of foot shock for 20 min (contextual cue exposure before shock association). Five days after the unpaired contextual cue session, mice were run in the standard unpredictable foot-shock session (approximately 20 unpredictable foot shocks, 0.75 mA, 500 ms) for 5 consecutive days as stated above, which included paired presentation of the contextual cues. Seven days after the fifth unpredictable foot-shock session, mice were placed back into the unpredictable foot-shock model, in which they received the visual and auditory contextual cues (house light and white noise) in the absence of foot shock for 20 min.

***In vivo* electrophysiology.** Neural activity was recorded using an Omniplex recording system (Plexon Instruments). Signals from each electrode in the array were referenced to ground, and recordings were performed in differential mode to subtract artefacts unrelated to neural activity. Acquired data was band-pass filtered between 0.1 and 8,000 Hz. Spike sorting was performed offline using Offline sorter (Plexon Instruments), as previously described[31,32]. In brief, discrimination of individual units was performed offline using principal component analysis to separate

individual units from the same electrode. In addition, auto- and cross-correlograms, firing characteristics, and inter-spike interval distributions were examined to ensure units were well isolated. In addition, timestamp data to signify the start and end of foot-shock sessions, and the delivery of light pulses to optical fibres were synchronized with electrophysiological data. Sorted waveforms were further processed in NeuroExplorer (Nex Technologies) to extract unit timestamps and relevant events. NeuroExplorer-extracted timestamps were exported to MATLAB for further data processing and statistical testing. Neuronal units were included in the data if the signal-to-noise ratio was high, and the mean firing rate was between 0.5 and 25 Hz during baseline recording periods. During the time epoch surrounding the individual delivered foot shocks, large shock artefacts were readily apparent. Although these were easily isolated and excluded from the analysed waveform data using offline spike sorting, neuronal firing responses in the 500–1,000 ms after foot-shock onset could not be reliably quantified. Thus, data collected during these time epochs were excluded from analysis. This represents an approximate loss of 0.8–1.66% of the collected data during the foot-shock session. Resulting data was binned in 30-s epochs to minimize the skewing of our results due to data lost by the shock artefacts. In addition, recording sites was verified histologically using electrolytic lesions at 200 μA for 5 s.

To identify units originating from vBNST projection neurons, 5-ms light pulses were delivered to the VTA to antidromically stimulate vBNST projection neurons that innervated the area. Light pulses were delivered in 10-s intervals for 20 trials starting 40 min after the end of the unpredictable foot-shock session. Recorded vBNST units were classified as light-responsive, and thus VTA-projecting, if they met both of the following two criteria: (1) the latency of the first spike after light stimulation onset was less than 20 ms for ≥20% of the trials; and (2) light-evoked and spontaneous waveform shapes had a correlation coefficient of >0.90. To compare light-evoked and spontaneous waveforms from units, light-evoked waveform characteristics were defined using the average waveform shape and average principal component values (PC1–3) of the first spike after photostimulation onset from each successful trial where a waveform was collected within 20 ms after light onset. This subset of light-evoked waveforms was then averaged together for a given unit, and compared to a subset of spontaneous, non-light-evoked waveforms that occurred immediately before the onset of light stimulations (pre-stimulation waveforms) and the first collected waveforms occurring after the 20-ms interval after the offset of photostimulations (post-stimulation waveforms). The correlation between each average waveform shape over the three time epochs (pre-stimulation, during stimulation and post-stimulation) was then calculated using Pearson's product-moment coefficient as well as their average principle component values.

VTA-projecting vBNST neuronal units were then further classified, dependent on their firing response to the foot-shock session into three categories: foot-shock session-excited, foot-shock session-inhibited, and foot-shock session-no effect. To clarify, foot-shock session-excited, foot-shock session-inhibited, and foot-shock session-no effect refers to the activity of a neural unit in response to the collective aversive experience, not to individual foot shocks. To assess the firing rate of a particular neuron, each spike from 10 min before the foot-shock session to 20 min after the end of the foot-shock session was binned into 30-s bins. Firing rate was then normalized to the mean firing rate during the 10-min before the start of the 20-min foot-shock session using z-scores. Neurons were classified as foot-shock-session-excited if their average z-score during the 20-min foot-shock session was greater than 1. Likewise, neurons were classified as foot-shock-session-inhibited if their average z-score during the shock session fell below −1. All other units in which the z-score did not exceed an absolute value of 1 during the 20-min foot-shock session were classified as no effect. Neural activity was recorded from the same mice during the cue exposure, foot shock, and cue re-exposure sessions, therefore we were able to record activity reliably from the same population of neurons during each of the three sessions.

Photostimulation and photoinhibition during the RTPP test. *Vglut2*$^{vBNST–VTA}$::ChR2, *Vgat*$^{vBNST–VTA}$::ChR2, *Vgat*^{VTA}::eNpHR3.0 and littermate controls were implanted with optical fibres above the VTA and were run in the RTPP test. See ref. 10 for further details.

Intra-VTA injection of antagonists and photostimulation during the RTPP test. A separate cohort of *Vglut2*$^{vBNST–VTA}$::ChR2 and *Vgat*$^{vBNST–VTA}$::ChR2 mice was unilaterally implanted with a 26-gauge cannula coupled to an optical fibre aimed above the VTA. All mice were placed in a custom-made place preference arena and were run in the RTPP test to achieve a baseline measurement. Two days after the baseline session, *Vglut2*$^{vBNST–VTA}$::ChR2 mice were injected with either 0.3 μl of vehicle (saline) or a cocktail of selective glutamate antagonists (0.1 μg AP5, 0.001 μg DNQX in saline), and *Vgat*$^{vBNST–VTA}$::ChR2 mice were injected with either 0.3 μl of vehicle (saline) or a selective $GABA_A$ antagonist (0.001 μg gabazine) into the VTA in a counter-balanced design (all drugs from Tocris). The injector needle (33-gauge steel tube, McMasters-Carr) extended approximately 1 mm past the cannula to ensure drug delivery 0.5 mm below the optical fibre. All mice were infused at a rate of 0.1 μl per minute. The injector remained in place for approximately 2 min after infusion to ensure proper diffusion of drug into the VTA. Immediately after the microinjection procedure, all mice were placed into the RTPP chamber. Mice had 2 days off in between each VTA microinjection.

Photostimulation of projections during open-field testing. *Vglut2*$^{vBNST–VTA}$::ChR2 and *Vglut2*$^{vBNST–VTA}$::control mice were examined in a custom-made open-field arena (25 × 25 × 25-cm white plexiglass arena) for 35 min. After a baseline period of 5 min, all mice received constant 20-Hz photostimulation. Immediately after the 20-min photostimulation epoch, all mice had a 10-min period in which they received no photostimulation. The centre zone was defined as the centre 156 cm^2 (25% of the entire arena). Corner zones were defined as the 39 cm^2 in each corner. The 35-min session was recorded with a CCD camera that was interfaced with Ethovison software (Noldus Information Technologies). Time spent in the corner and the centre of the open-field apparatus was recorded. Heat maps and post-acquisition processing were conducted in MATLAB (Mathworks).

Photostimulation of projections during sucrose self-administration. *Vglut2*$^{vBNST–VTA}$::ChR2 and *Vglut2*$^{vBNST–VTA}$::control mice with optical fibres implanted above the VTA were first food restricted to 90% of their free-feeding weight. They were then placed in standard mouse operant chambers to nose poke for a 15% (w/v) sucrose solution on a fixed-ratio 1 schedule in a 30-min session. Once stable nose-poking behaviour for 15% sucrose was observed (approximately 100 active nose pokes on at least two consecutive days), all mice received constant 20-Hz photostimulation during the entire 30-min sucrose session.

Optical self-stimulation of *Vgat*$^{vBNST–VTA}$::ChR2 projections. *Vgat*$^{vBNST–VTA}$::ChR2 and *Vgat*$^{vBNST–VTA}$::control mice with optical fibres implanted above the VTA were trained in one 30-min session to nose poke on a fixed-ratio 1 schedule for optical self-stimulation of the *Vgat*$^{vBNST–VTA}$::ChR2 projections in standard mouse operant chambers (Med Associates). Each nose poke resulted in a single 3-s 20-Hz optical pulse train. After the 1-day 20-Hz training session, mice were run daily at each photostimulation frequency (1, 5, 10, 20 and 40 Hz) in a counter-balanced design.

Optical self-inhibition of *Vgat*^{VTA}::eNpHR3.0 neurons. *Vgat*^{VTA}::eNpHR3.0 and *Vgat*^{VTA}::control mice with optical fibres implanted above the VTA were trained in one 30-min session to nose poke on a fixed-ratio 1 schedule for photoinhibition of VTA GABAergic cell bodies in standard mouse operant chambers as described above (Med Associates).

Photostimulation and photoinhibition during the EPM test. *Vgat*$^{vBNST–VTA}$::ChR2, *Vgat*^{VTA}::eNpHR3.0, *Vgat*^{VTA}::control, and *Vgat*$^{vBNST–VTA}$::control mice were run in the EPM test to assay anxiety-like behaviour. Activity and location was recorded for 5 min (baseline). After this 5-min baseline period, *Vgat*$^{vBNST–VTA}$::ChR2 and *Vgat*$^{vBNST–VTA}$::control mice received constant 20-Hz photostimulation for 5 min, whereas *Vgat*^{VTA}::eNpHR3.0 and *Vgat*^{VTA}::control mice received constant inhibition for 5 min. Immediately after the 5-min photostimulation or photoinhibition epoch, all mice had a 5-min period in which they received no light delivery.

Photostimulation during foot-shock, freezing and anxiety-like behaviour. *Vgat*$^{vBNST–VTA}$::ChR2 and *Vgat*$^{vBNST–VTA}$::control mice with optical fibres implanted above the VTA were run in a modified foot-shock test as described earlier. In brief, mice were placed into sound-attenuated mouse chambers (Med Associates) for a 5-min baseline period. After the 5-min baseline period, a house light and white noise were activated and mice received the same foot-shock protocol as described above. Furthermore, during the 20-min shock session, all mice received constant 20-Hz photostimulation. A separate cohort of mice (*Vgat*$^{vBNST–VTA}$::ChR2 and *Vgat*$^{vBNST–VTA}$::control) received constant 20-Hz photostimulation of this pathway in the absence of foot shock. Immediately after the 20-min foot-shock and photostimulation epoch, all mice had a 5-min period in which they received no foot shock or photostimulation while still exposed to contextual cues, to assay freezing behaviour. Freezing was defined as the total lack of any movement, except respiration, for a period of 2 s. The 30-min test session was recorded with a CCD camera that was interfaced with Ethovision software (Noldus Information Technologies). The time frozen during the 5-min period immediately after the foot shock and photostimulation session was recorded. Approximately 3 h after the foot-shock and photostimulation session or just the photostimulation session in the absence of foot shock, mice were run on the EPM test to assay anxiety-like behaviour for 5 min.

31. Roitman, M. F., Wheeler, R. A. & Carelli, R. M. Nucleus accumbens neurons are innately tuned for rewarding and aversive taste stimuli, encode their predictors, and are linked to motor output. *Neuron* **45,** 587–597 (2005).
32. Tye, K. M. & Janak, P. H. Amygdala neurons differentially encode motivation and reinforcement. *J. Neurosci.* **27,** 3937–3945 (2007).